ACS APPLIED MATERIALS & INTERFACES
Research Article
www.acsami.org

Nanocrystallized CdS beneath the Surface of a Photoconductor for Detection of UV Light with Picowatt Sensitivity

Keng-Te Lin,[†] Hsuen-Li Chen,*[,†] Yu-Sheng Lai,*[,‡] Yu-Lun Liu,[†] Yi-Chuan Tseng,[†] and Cheng-Hsi Lin[†]

[†]Department of Materials Science and Engineering, National Taiwan University, 1, Sec. 4, Roosevelt Road, Taipei, Taiwan
[‡]National Nano Device Laboratories, National Applied Research Laboratories, 26, Prosperity Road I, Hsinchu, Taiwan

Supporting Information

ABSTRACT: In this study, we demonstrated that the improvement of detection capability of cadmium sulfide (CdS) photoconductors in the ultraviolet (UV) regime is much larger than that in the visible regime, suggesting that the deep UV laser-treated CdS devices are very suitable for low-light detection in the UV regime. We determined that a nanocrystallized CdS photoconductor can behave as a picowatt-sensitive detector in the UV regime after ultra-shallow-region crystallization of the CdS film upon a single shot from a KrF laser. Photoluminescence and Raman spectra revealed that laser treatment increased the degree of crystallization of the CdS and led to the effective removal of defects in the region of a few tens nanometers beneath the surface of CdS, confirming the result by the transmission electron microscopy (TEM) images. Optical simulations suggested that UV light was almost completely absorbed in the shallow region beneath the surface of the CdS films, consistent with the observed region that underwent major crystal structure transformation. Accordingly, we noted a dramatic enhancement in responsivity of the CdS devices in the UV regime. Under a low bias voltage (1 mV), the treated CdS device provided a high responsivity of 74.7 A W^{-1} and a detectivity of 1.0×10^{14} Jones under illumination with a power density of 1.9 nW cm^{-2}. Even when the power of the UV irradiation on the device was only 3.5 pW, the device exhibited extremely high responsivity (7.3×10^5 A W^{-1}) and detectivity (3.5×10^{16} Jones) under a bias voltage of 1 V. Therefore, the strategy proposed in this study appears to have great potential for application in the development of CdS photoconductors for picowatt-level detection of UV light with low power consumption.

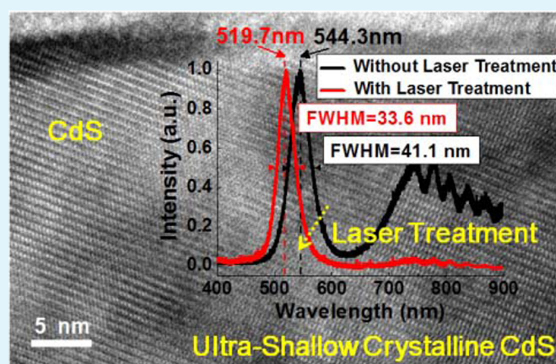

KEYWORDS: *cadmium sulfide (CdS), ultra-shallow-region crystallization, KrF excimer laser, photoconductor, picowatt-sensitive UV detector, low power consumption*

INTRODUCTION

There is currently great interest in the development of stable, highly sensitive detectors of ultraviolet (UV) light because of their applications in, for example, monitoring of environmental UV radiation, astronomical studies, fabrication of integrated circuits (ICs), and biological and chemical sensing.[1−5] The monitoring of UV radiation in the environment has become a global issue because increased amounts of UV radiation reaching the Earth's surface may be dangerous to human health.[6] In addition, precise monitoring of the intensity of UV light is important during the optical lithography processes used in IC fabrication.[7]

In general, photodetectors can be divided into two distinct types based on their operation principles: junction-type detectors[2,4,8−11] and photoconductors.[12,13] Junction-type devices are more commonly employed in photodetection. Crystalline silicon (Si)-based junction-type detectors are usually used to detect light over broad spectral regimes.[9,11] Nevertheless, Si-based photodetectors have their limitations; for example, the processes used to prepare Si−based devices are complicated and their resulting quantum efficiencies are not sufficiently high when applying a low bias voltage (on the order of millivolts).[14] Moreover, most of the incident UV light cannot reach the junction within a Si−based devices because Si absorbs strongly in the UV regime; for example, the absorption coefficient of Si[15] at a wavelength of 320 nm is approximately 1.3×10^6 cm^{-1}. Therefore, the short penetration depth within Si limits the photoresponse of Si−based photodetectors in the UV regime.

Recently, a new generation of junction-type UV photodetectors has emerged, based on wide−bandgap semiconductors, including silicon carbide (SiC)[8,16] and zinc oxide (ZnO).[1,2,4] Indeed, significant improvements in performance have been achieved when using SiC−based UV photodetectors. Such devices offer not only remarkable operating stability but also good performance in the UV regime.[16] Nevertheless, the growth of SiC wafers on a large scale with good crystallinity and

Received: August 7, 2014
Accepted: October 24, 2014
Published: November 6, 2014

 © 2014 American Chemical Society

the subsequent fabrication of SiC-based photodetectors both remain complicated and expensive.

ZnO is a common material within optoelectronic devices that operate in the UV regime.[4,17−21] Compared with other wide−bandgap materials, ZnO can be synthesized using solution−based techniques, thereby enabling the ready fabrication of devices over large areas at low cost. Recently, special ZnO nanostructures, including nanowires, nanosheets, and hollow nanospheres,[22] have been investigated extensively to increase the harvesting of incident light. The surface-to-volume ratios of these nanostructured ZnO devices are much higher than those the bulk ZnO structures.[4,17,18] In general, these nanostructured devices should tolerate large applied bias voltages and provide large dark current densities and long response times (up to several seconds).[17,18,22]

The other type of device that can be used for light detection is a photoconductor. The processes for preparing photoconductors are simple and cheap. Ideally, photoconductor devices should absorb strongly to generate a large number of light−induced carriers when the light is applied incident to the photoconductor material. Most photoconductors comprise semiconductor materials; for example cadmium sulfide (CdS),[12] zinc sulfide (ZnS),[23] and lead sulfide (PbS).[24] In general, the resistance of a photoconductor is large in the absence of light. When light is applied to a photoconductor, excess carriers are generated; they flow along the direction of the supplied voltage, thereby changing the material's conductivity.[25] The ability to dramatically enhance the difference in conductivity between dark and illuminated states remains a challenge.

CdS is a promising and inexpensive photoconducting material. Previous studies have demonstrated that the absorption coefficient and carrier mobility of CdS are larger than those of other photoconductor materials, such as ZnO and ZnS.[15,26,27] In addition, because the band gap energy of CdS is approximately 2.4 eV,[26] it is a very attractive material for photodetectors operating in the visible regime. Moreover, the photoresponse spectra of CdS materials match well with the spectrum of solar radiation in the visible regime, allowing CdS to be investigated for use in the field of thin film solar cells.[28−30] There are many factors that affect the conductivity of CdS films, including the grain size, the band gap energy, the defect density, and the nature of any doping species. Several groups have successfully manufactured crystalline CdS and have demonstrated that thermal[31,32] and laser[12,33] treatment can improve the conductivity of and decrease the number of defects in CdS films.[31,32] Moreover, in our previous study,[12] we have demonstrated that a CdS device treated with many shots from a KrF laser at a suitable power density could exhibit improved photoresponse in the visible regime. To the best of our knowledge, however, few studies have focused on the preparation of CdS-based photodetectors that operate in the UV regime.

In this study, for the first time, we found that the improvement of detection capability of CdS photoconductors in the UV regime is much larger than that in visible regime after deep ultraviolet (DUV) laser treatment. Here, we applied a KrF excimer laser to treat the surfaces of CdS[34] photoconductors to obtain systems capable of detection of UV light with extremely high sensitivity (for details, please see the Methods in the Supporting Information). Indeed, a single shot of KrF laser treatment alone provided sufficient energy to improve the crystallization of CdS devices significantly within the ultra-shallow region beneath the surface. Our laser-treated devices possessed good surface crystallinity, allowing the effective generation and collection of light-induced carriers under light of picowatt intensity in the UV regime.

RESULTS AND DISCUSSION

To compare the optical behaviors of CdS and conventional Si based devices, we used the three-dimensional finite-difference time-domain (3D-FDTD) and optical thin-film methods to analyze light of distinct wavelengths propagating through the CdS and Si, respectively (for details, please see Figure S2 in the Supporting Information). We first set plane waves propagating from 400 nm above the air−material (CdS or Si) interface; we then set some detectors above and below the surface of the material to monitor the surface reflection and the light transmission into the material, respectively. The CdS film exhibited superior absorption characteristics in the UV regime; the absorption coefficient of CdS[15] at the wavelength of the

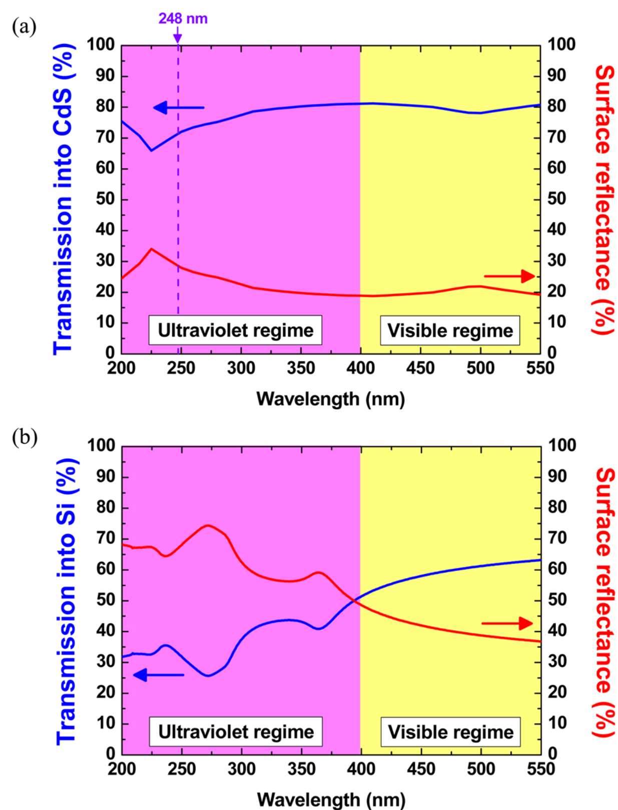

Figure 1. Simulation of light propagating on CdS and Si based devices. (a) Surface reflectance and light transmission into CdS at distinct wavelengths. (b) Surface reflectance and light transmission into Si at distinct wavelengths.

Table 1. Penetration Depths of the Light Propagating into the CdS as the Intensities Dropped to 50%, 36.79% (e^{-1}), 10%, and 1% at the Distinct Wavelengths

	penetration depth (nm) at given intensity			
wavelength (nm)	50%	36.79% (e^{-1})	10%	1%
248	6	9	27	60
325	11	17	68	145
365	14	22	90	195
532	24	39	216	469

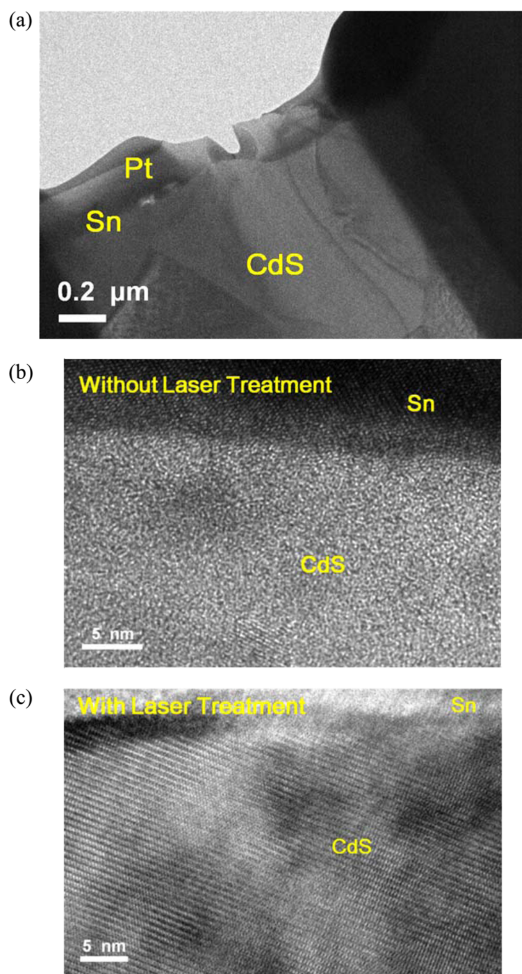

Figure 2. TEM images of CdS photoconductors (a) at low magnification and (b, c) at high magnification (b) before and (c) after KrF laser treatment.

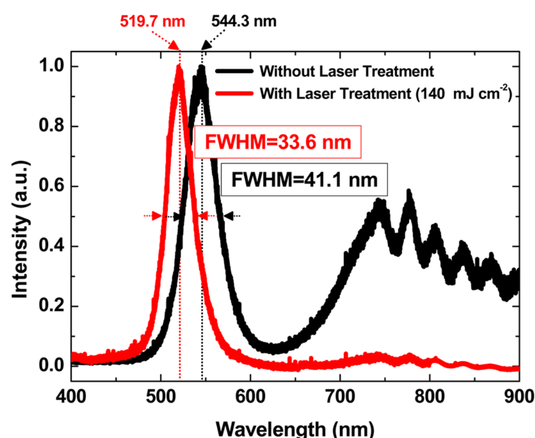

Figure 3. PL spectra of CdS sample before (black curve) and after (red curve) laser treatment.

KrF laser (248 nm) was 7.3×10^5 cm^{-1}. As displayed in Figure 1a, the surface reflection at the wavelength of 248 nm was less than 30%, and therefore, more than 70% of light would propagate into the CdS film to be absorbed. Furthermore, most of the DUV light was absorbed in the ultrashallow region beneath the surface of CdS (ca. 60 nm) (as displayed in Table 1). Therefore, we would predict that the major transformations

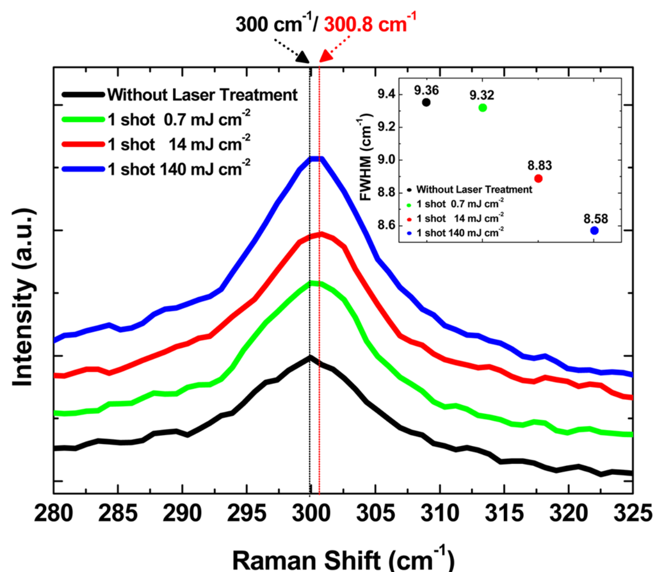

Figure 4. Measured Raman spectra of CdS samples before and after a single shot from a KrF laser at various intensities.

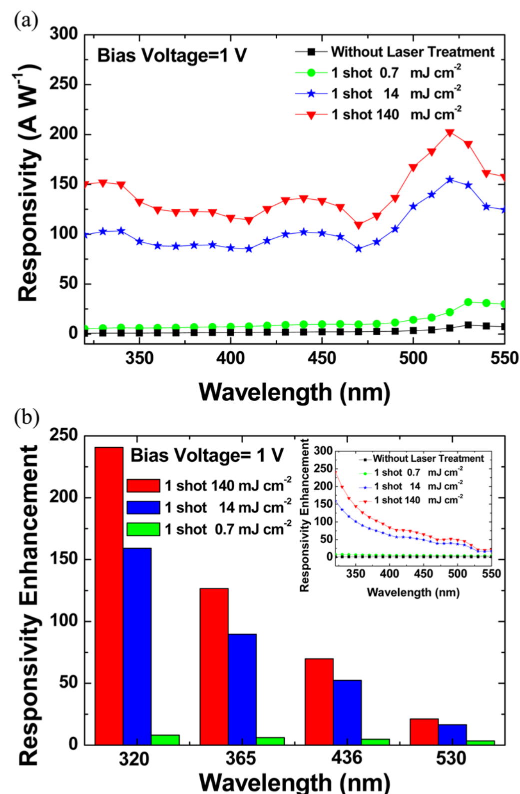

Figure 5. (a) Photocurrent responses of CdS photoconductors before and after KrF laser treatment, measured under an applied bias voltage of 1 V and illumination with light at wavelengths in the range from 320 to 550 nm. (b) Responsivity enhancements at different wavelengths for laser-treated CdS devices, normalized with respect to the responsivity of the device prepared without laser treatment.

in crystal structure occur around the ultrashallow region beneath the surface of CdS photoconductor when using a KrF laser as the laser treatment source.[12] Moreover, the surface reflection from the UV to visible regime is all ca. 20% due to the similar refractive index in these regimes.[15] Therefore, the light could be sufficient transmission into CdS even without

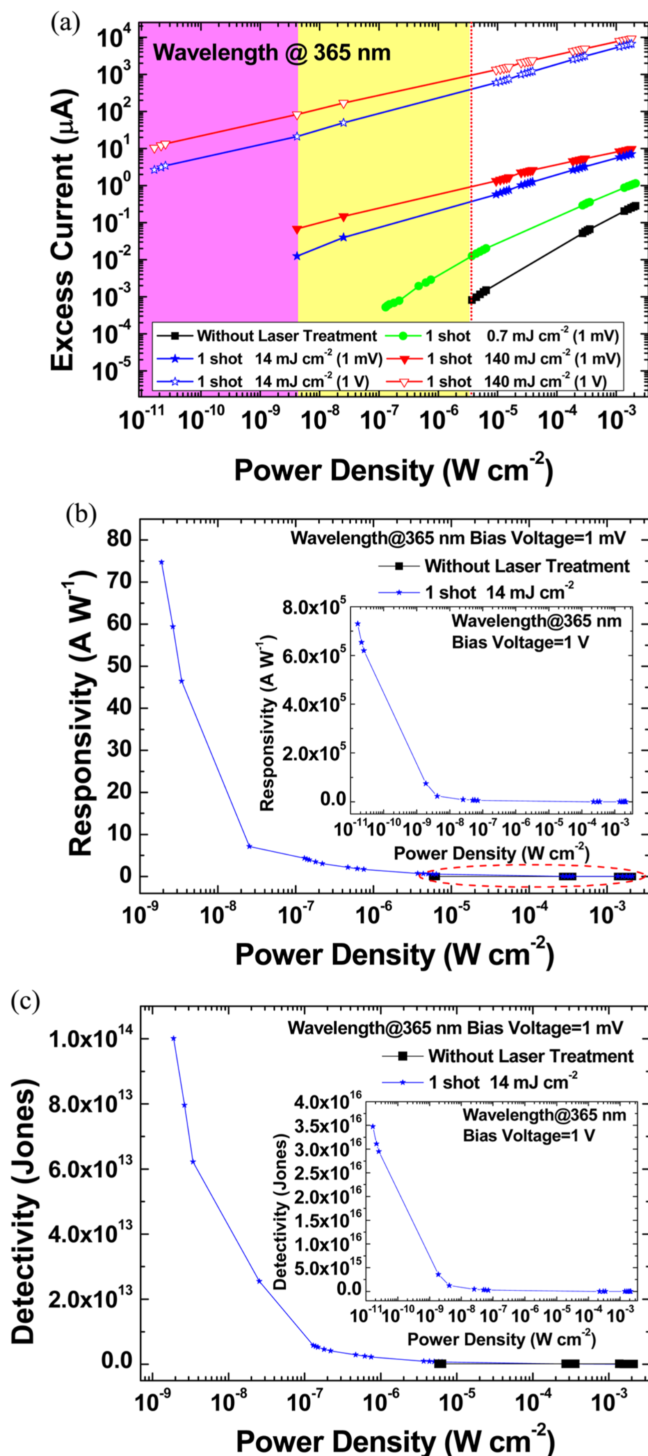

Figure 6. (a) Correlation between excess current and illumination power density. (b) Responsivity of the laser-treated CdS device plotted with respect to the illumination power density at a bias voltage of 1 mV. Inset: Responsivity plotted with respect to the illumination power density at a bias voltage of 1 V. (c) Detectivity of the laser-treated CdS device plotted with respect to the illumination power density at a bias voltage of 1 mV. Inset: Detectivity plotted with respect to the illumination power density at a bias voltage of 1 V.

introducing any antireflective coating or textured micro/nano structure. In contrast, as displayed in Figure 1b, the Si performed large surface reflection loss of ca. 65% in the UV regime and ca. 40% in the visible regime that the antireflective structures would be very important to improve the light harvesting. Furthermore, we investigated the optical behaviors of incident light with the wavelengths of 248, 325, 365, and 532 nm on the absorption of CdS films. Table 1 displays the penetration depths of the light propagating into the CdS as the intensities dropped to 50%, 36.79% (e^{-1}), 10%, and 1% at the distinct wavelengths. In the UV regime, the intensity of light was reduced to 10% at the depth only ca. 70 nm below the air–CdS interface. In the visible regime, however, the light could propagate to the depth of 216 nm with the 10% intensity of incident light. Thus, UV light would be almost completely absorbed within the shallow region beneath the surface of the CdS film. We predicted, therefore, that treatment with a KrF laser would locally anneal the ultrashallow region beneath the surface of CdS, providing CdS photodetectors with good surface crystallization characteristics for the harvesting of UV light.

In general, structural defects in CdS introduce trap centers that lead to recombination of free carriers under illumination with light. Decreasing the number of defects would, therefore, increase the electron transport efficiency and further enhance the photocurrent. The KrF excimer laser is a deep-ultraviolet (DUV) laser (λ = 248 nm) having high photon energy and short pulse duration. With the only one shot of laser treatment, the DUV light was almost absorbed by CdS within the depth of ca. 60 nm. Consequently, the major transformations in crystal structure occur in a few tens nanometers region beneath the surface of CdS. Figure 2 displays TEM images of CdS devices before and after laser treatment. In the low-magnification image in Figure 2a, we observe that the deposited Pt layer successfully protected the morphology of the CdS film during the focused ion beam (FIB) process and that of the Sn electrode on the surface of the CdS film. Figure 2b, c displays the high-resolution TEM (HR-TEM) images of the CdS device before and after KrF laser treatment, respectively. Prior to laser treatment, dislocation and noncrystallization were evident near the interface between the CdS film and the electrode. Laser treatment with a single shot of KrF laser at an intensity of 140 mJ cm^{-2} increased the degree of crystallization of the CdS film and also removed its defects in the region of several tens nanometers beneath the surface of CdS. Accordingly, we suspected that the excess carrier lifetimes of the laser–annealed CdS films would be enhanced effectively. Consequently, when we illuminated the CdS devices with light, the excess carriers generated in the CdS films would migrate with a lower degree of carrier recombination, implying that the conductivity and photocurrent would also be improved.

Next, we prepared samples by irradiating devices with a single shot from a KrF laser at power densities of 0.7, 14, and 140 mJ cm^{-2}. Figure 3 and Figure 4 display the measured PL and Raman spectra, respectively, of the CdS devices, with and without laser annealing, that we used to analyze the crystallization characteristics of the CdS films. And we also compared these results with TEM images (Figure 2) to confirm the degree of crystallization of the CdS film and the reduction of defect densities.

We measured the PL spectra of the CdS samples at room temperature, using a He–Cd laser (wavelength: 325 nm) as the excitation source. Prior to laser treatment [Figure 3 (black curve)], the spectrum displayed a near-band-edge emission peak located near 544 nm and a broadband and obvious emission in the near-infrared (NIR) regime; that is, we detected deep-level and trap-state emissions. After a single shot of laser

Table 2. Comparison of the performance (responsivity, detectivity, applied voltage) of recently reported photodetectors of UV light

authors	device type	material	responsivity (A W^{-1})	detectivity (Jones)	applied voltage (V)	ref
E. S. Ates et al.	photodiode (junction type)	ZnO	ca. 0.14 (@ 370 nm)		2	4
L. Hu et al.	photoconductor (nanobelt)	ZnS/ZnO	5×10^5 (@ 320 nm)		5	18
X. Wang et al.	photodiode (junction type)	ZnO	35.9 (@ 350 nm)		3	22
T. S. Lin et al.	photodiode (p-i-n)	ZnO	0.102 (@ 360 nm)	3.08×10^{11}	−5	10
Z. Li et al.	photodiode (p-n)	Si	ca. 0.12 (@ 320 nm)		−1	11
Y. Koda et al.	photodiode (p-n)	Si	ca. 0.215 (@ 300 nm)		2	9
F. Yan et al.	photodiode	SiC	ca. 0.3 (@ 320 nm)	ca. 10^{15}	−1	16
D. Li et al.	photodiode (junction type)	GaN	ca. 4 (@ 355 nm)		5	40
B. Butun et al.	photodiode (p-i-n)	GaN	ca. 0.23 (@ 356 nm)		5	41
this work	photoconductor	CdS	32.2 (@ 320 nm)	4.3×10^{13} (@ 320 nm)	0.001	
			74.7 (@ 365 nm)	1×10^{14} (@ 365 nm)		
			7.8×10^4 (@ 320 nm)	3.7×10^{15} (@ 320 nm)	1	
			7.3×10^5 (@ 365 nm)	3.5×10^{16} (@ 365 nm)		

light at an intensity of 140 mJ cm^{-2} [Figure 3 (red curve)], the peak wavelength in the PL spectrum appeared near 520 nm. This blue−shift of the emission band agrees with that reported by Tsai et al.,[35] who found that it corresponded with an increased CdS grain size and a decrease in the number of defects. In addition, the full width at half-maximum (fwhm) of the PL emission band of the laser−treated sample (33.6 nm) was much narrower than that of the CdS sample that had not been subjected to laser treatment (41.1 nm). Thus, a single shot of laser treatment suppressed the NIR emission and led to a blue-shift of the PL emission peak, suggesting a significant decrease in defect density and improved crystallization of the CdS film.[35]

Raman spectroscopic analysis confirmed the crystallization characteristics of our CdS devices. Figure 4 presents the measured Raman spectra of CdS samples (both with and without KrF laser treatment) recorded using a solid state laser (wavelength: 532 nm) as the excitation source. In a previous report,[36] the Raman spectrum of single-crystalline CdS exhibited a signal for the 1 longitudinal optical (LO) mode at 305 cm^{-1}; moreover, the intensity of this mode is much higher than that of the other longitudinal optical mode, implying that the 1 LO mode is more sensitive to the crystallization characteristics of CdS. Therefore, in this present study we measured the micro−Raman spectra of CdS samples, with focus on the 1 LO mode region (Figure 4). The 1 LO peak for the film prepared without laser treatment was centered at 300 cm^{-1}, a lower value than that of the single−crystalline CdS. This shift, according to Chuu et al., is due to the small dispersion of the LO mode phonon wave vectors in polycrystalline films.[36] We found, however, that the position of the 1 LO peak shifted slightly, to 300.8 cm^{-1}, for the sample that had been subjected to a single shot of laser treatment at a power density of 140 mJ cm^{-2}. In addition, the FWHMs of the 1 LO peaks in the Raman spectra decreased from 9.36 cm^{-1} initially to 8.58, 8.83, and 9.32 cm^{-1} after single-shot laser treatment at power densities of 140, 14, and 0.7 mJ cm^{-2}, respectively (inset to Figure 4). We attribute the slight shifts of the 1 LO peaks and the decreases in the FWHMs after laser treatment to the enhanced degrees of crystallization of the CdS films and their decreased defect densities.[37]

Although the PL spectra revealed significant differences between the samples before and after laser treatment, their Raman spectra were quite similar. We had, however, recorded the PL and Raman spectra of the CdS devices using laser excitation at wavelengths of 325 and 532 nm, respectively. As displayed in Table 1, incident light having a wavelength 325 nm would be absorbed almost completely within a region of approximately 145 nm beneath the air−CdS interface. In contrast, incident light having a wavelength of 532 nm would propagate through a region of greater than 465 nm beneath the air−CdS interface (Table 1). Accordingly, the resulting absorption region in the CdS film at a wavelength of 532 nm was much larger than that at 325 nm. Therefore, we suggest that the measured PL signals after excitation by the laser at a wavelength of 325 nm would provide more crystallization information close to the surface of the CdS film. According to Table 1, most of the energy received from the single-shot KrF laser irradiation was absorbed within the region of approximately 60 nm beneath the air−CdS interface. Consequently, the information from the TEM image (Figure 2) and the PL signals confirmed that the degree of crystallization had improved and the defect density had decreased effectively in the shallow region beneath the surface of the CdS film after a single shot from the KrF laser.

To investigate the effect of laser treatment on CdS photoconductors, we measured the photoresponses of devices that had been irradiated with single shot from a KrF laser at power densities of 0.7, 14, and 140 mJ cm^{-2}. Figure 5a displays the photocurrent responses of the CdS photoconductors before and after laser treatment when applying a bias voltage of 1 V and illuminating with light from a Xe lamp through a monochromator at wavelengths in the range from 320 to 550 nm. The CdS devices prepared without laser treatment exhibited peak responsivity (ca. 8.9 A W^{-1}) at a wavelength of 530 nm, with very low responsivity over the entire spectral region. After laser treatment, the responsivity of the CdS devices increased dramatically over the entire wavelength range—especially in the UV regime. Moreover, gradually increasing the power density of the laser to 140 mJ cm^{-2} led to a corresponding gradual increase in responsivity.

The inset to Figure 5b presents the responsivities of the laser−treated CdS devices normalized with respect to the responsivity of the corresponding device prepared without laser treatment. Here, we selected wavelengths of 320, 365, 436, and 530 nm to observe the enhancements in responsivity. We chose these wavelengths for the following reasons: UVB radiation, which possesses wavelengths in the range between 280 and 320 nm, is dangerous to the human body; light having wavelengths of 365 and 436 nm is commonly used in conventional I-line/G-

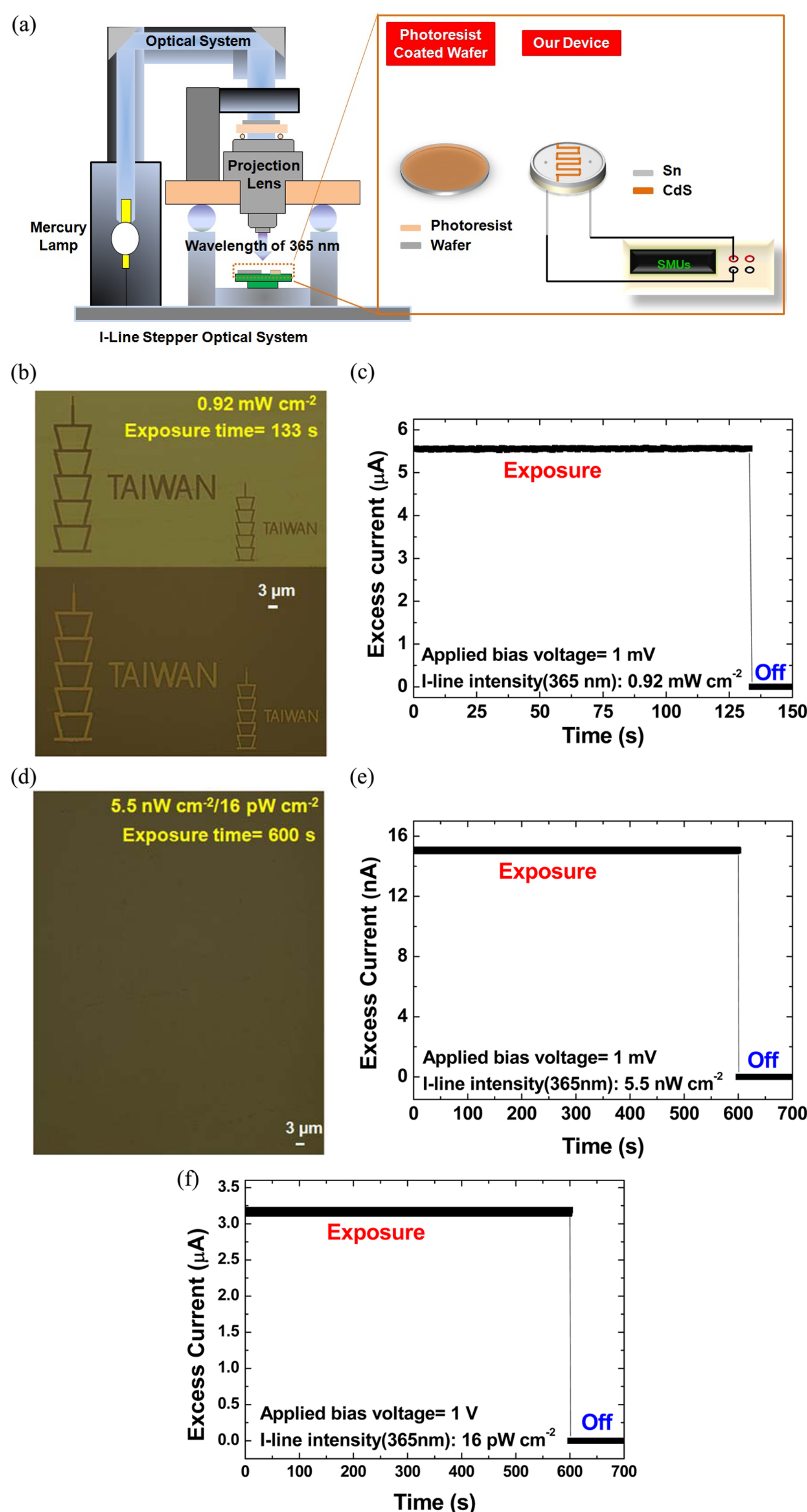

Figure 7. (a) Schematic representation of the experimental setup used to test the detection ability of photoresist and laser−treated CdS devices under UV light of low intensity. (b) Photograph of patterns (after development), recorded by the photoresist at a power density of 0.92 mW cm^{-2} for an exposure time of 133 s. (c) Plot of excess current with respect to time for the CdS device; the light intensity (0.92 mW cm^{-2}) could be determined from the photocurrent output. (d) Photograph of the photoresist (after development) that had been exposed to light of low power density (5.5 nW cm^{-2} or 16 pW cm^{-2}) for a long exposure time 600 s. (e, f) Excess current of the laser−annealed CdS, plotted with respect to time, measured under a light intensity of (e) 5.5 nW cm^{-2} when applying a bias voltage of 1 mV and (f) 16 pW cm^{-2} when applying a bias voltage of 1 V.

line optical lithography; in the absence of laser−treatment, the CdS device exhibited peak responsivity at a wavelength of 530 nm. We observed that the laser−treated devices exhibited enhancements in responsivity at each of these wavelengths; the

enhancement in responsivity at 530 nm was, however, much less than that at 320 nm. For example, after treatment with a single shot of laser light at a power density of 140 mJ cm^{-2}, the enhancements in responsivity at wavelengths of 530, 436, 365, and 320 nm were 22-, 70-, 125-, and 240-fold, respectively, relative to that of the device that had not been subjected to laser treatment. Thus, the enhancements in responsivity in the UV regime were much larger than those in the visible regime.

According to our material analyses and optical simulations, the major transformation in crystal structure induced by KrF laser treatment occurred in the ultrashallow region beneath the surface of each CdS device. In addition, incident light at wavelengths of 320 (UV) and 530 (visible) nm would be almost completely absorbed at depths of approximately 100 and 400 nm, respectively, below the air−CdS interface. The high absorption region within the CdS devices in the UV regime would, therefore, overlap to a greater degree with the major region of crystal structure transformationthan that in the visible regime. If the laser-treated CdS devices were to be illuminated with UV light (rather than visible light), a greater number of excess carriers would be generated in the CdS films with a low degree of carrier recombination, implying a large enhancement in photoresponsivity. Furthermore, the crystallization characteristics of CdS can be improved upon gradually increasing the power density of the light from the KrF laser. We found, however, that irradiation from the KrF laser not only decreased the degree of dislocation and enhanced the crystallization of the CdS film but also induced laser ablation. Thus, in this study, the optimal conditions for the laser treatment process included a single shot of laser light at a power density of 140 mJ cm^{-2}.

To compare the photocurrents provided by devices that had been treated under various conditions, we define the excess current as the difference between the photocurrent and the dark current; these values can be obtained from the measurement data of devices under illumination with incident light of various intensities and wavelengths. Figure 6a displays the excess currents recorded while applying biases of 1 mV and 1 V at a wavelength of 365 nm. The excess currents of the CdS devices obtained after laser treatment were much higher than those of the device prepared without laser treatment, consistent with the data in Figure 5a. Notably, the excess current from the device obtained after a single shot of laser treatment at a power density of 14 mJ cm^{-2} was close to that from the device treated at a laser intensity of 140 mJ cm^{-2}, implying the possibility of decreasing the power density during the laser treatment process. When applying a bias voltage of 1 mV, the enhancements in excess current of the devices treated with single shot of laser light at 14 and 140 mJ cm^{-2} were approximately 500−fold and 3 orders of magnitude, respectively, relative to that of the device that had not been subjected to laser treatment. As presented in Figure 6a, for an excess current of less than 1 nA, the detectable power density was limited at approximately 5 μW cm^{-2} for the device that had not been subjected to laser treatment. After laser treatment, the excess current of the device increased significantly, even when the incident power density was less than 4 nW cm^{-2}. Moreover, when applying a bias voltage of 1 V, the device that had been treated with laser light at a power density of 14 mJ cm^{-2} exhibited a notable excess current greater than 2.6 μA at an incident power density of 16 pW cm^{-2}. Notably, because the active area of the device was 0.22 cm^2, the light power irradiated on the device was only 3.5 pW. Consequently, even when the power density during laser treatment was as low as 14 mJ cm^{-2}, the resulting CdS devices were still able to detect ultralow levels of UV light.

To further evaluate the performance of the CdS devices, we measured their responsivities (R, A W^{-1}) and detectivities (D^*, cm $Hz^{1/2}$ W^{-1} or Jones), which can be expressed using eqs 1 and 2,[38] respectively

$$R = \frac{J_{ph}}{P_{light}} \tag{1}$$

$$D^* = \frac{R}{\sqrt{2qJ_d}} = \frac{J_{ph}}{P_{light}\sqrt{2qJ_d}} \tag{2}$$

where J_{ph} is the photocurrent density, P_{light} is the incident light power density, q is the absolute value of electronic charge, and J_d is the dark current density. On the basis of the measured photocurrents, dark currents, and incident−light power densities, we determined the responsivities (Figure 6b) and detectivities (Figure 6c) of the CdS device treated with a single shot of laser light at 14 mJ cm^{-2} at a wavelength of 365 nm. As the measured data displayed as the oval-shaped dash line in Figure 6b, the responsivities of the treated devices reveal more than ten times to two-orders-of-magnitude enhancements than those of devices without laser treatment when the devices illuminated with light intensity in the range between 5 μW cm^{-2} and 1.9 mW cm^{-2} (please see the Supporting Information, Figure S3). For example, under an incident power density of 5 μW cm^{-2} and a bias of 1 mV, the responsivity of the device improved dramatically after laser treatment, from 0.001 to 0.57 A W^{-1}. We also measured the responsivities and detectivities of the devices under an applied bias voltage of 1 V (insets to Figure 6b, c, respectively). Under illuminating light at a power density of only 1.9 nW cm^{-2}, the responsivities of the laser−annealed devices were 74.7 and 7.5 $\times$ 10^4 A W^{-1} under bias voltages of 1 mV and 1 V, respectively. Notably, under an applied bias voltage of 1 V, the responsivity of the laser−treated device was remarkable—7.3 $\times$ 10^5 A W^{-1}—at an incident power density of only 16 pW cm^{-2}.

According to eq 2, the responsivity (R) and dark current density (J_d) are the major factors influencing the detectivity of a photodetector. Figure 6c reveals that the detectivity increased significantly, from 1 $\times$ 10^{11} to 1 $\times$ 10^{14} Jones, in the laser−treated device when we decreased the incident power density from 2 mW cm^{-2} to 1.9 nW cm^{-2}. As exhibited in the insets to Figure 6b, c, the responsivity and detectivity both increased when applying a bias voltage of 1 V. For example, the laser−annealed CdS device could still provide a responsivity of 7.3 $\times$ 10^5 A W^{-1} and a detectivity of 3.5 $\times$ 10^{16} Jones at an incident power density of 16 pW cm^{-2}. Moreover, considering the power consumption of photodetectors, a low bias voltage of 1 mV would be desirable. In this study, under a low incident power density of 1.9 nW cm^{-2}, the laser-annealed CdS device could provide a responsivity of 74.7 A W^{-1} and a detectivity of 1.0 $\times$ 10^{14} Jones when biased at only 1 mV. In addition, we also measured the excess currents and evaluated the responsivities and detectivities of CdS devices at a wavelength of 320 nm (see Figure S4 in the Supporting Information). The electrical behavior of the CdS devices at a wavelength of 320 nm was similar to that at a wavelength of 365 nm. Moreover, the measured rise and fall times of the laser-annealed CdS device were only approximately 40 and 70 ms, respectively; that is, they were much faster than those of ZnO-based[4,18] UV photodetectors (see Figure S5 in the Supporting Information).

In addition, the electrical behaviors of the treated CdS devices were also stable and reproducible under UV illumination (see Figure S6 in the Supporting Information). Therefore, the strategy proposed herein has great potential for the detection of ultralow levels of UV light with low power consumption.

Table 2 compares the performance of the CdS devices prepared in this study with that of other photodetectors for UV light. Although several recently reported photodetectors exhibit responsivities in the range from 0.1 to 5×10^5 A W^{-1}, most devices exhibiting high responsivity require operation under large bias voltages.[10,18,22,39−41] In addition, the high detectivities of SiC-based detectors result in good detection capabilities as a result of low dark−current densities; such SiC-based detectors are, however, generally expensive and possess relatively low responsivities, thereby limiting their applicability for the detection of ultra-low-intensity UV light. The laser-treated CdS devices we prepared in this study achieved very high responsivities and detectivities under low-light conditions (1.9 nW cm^{-2}), even when applying a bias voltage of only 1 mV. In addition, under a common bias voltage of 1 V, this device exhibited a high responsivity (7.3×10^5 A W^{-1}) and a high detectivity (3.5×10^{16} Jones) under conditions of extremely low light (16 pW cm^{-2}).

Figure 7a displays a schematic representation of the experimental setup that we used to test the detection ability of a CdS device. We used the light source from a contact aligner (I-line, 365 nm) to test the device's UV−light detection capability. For comparison, we also simultaneously tested the low-light performance of a conventional photoresist (TOK ip3650) used in standard optical lithography processes. This photoresist is a highly sensitive toward the low-intensity UV light applied in IC processing. In general, a photoresist requires a certain exposure time to complete its chemical reactions under low-intensity UV light; thus, a photochemical reaction is required to ensure sufficient "dosage accumulation" in the resist. Figure 7b displays the pattern recorded by the photoresist at a power density of 0.92 mW cm^{-2} with an exposure time of 133 s. After applying these exposure conditions and subsequent development, the photoresist could present the design patterns. In addition, the photocurrent output from the laser-treated CdS device allowed us to record the light intensity of the contact aligner. As displayed in Figure 7c, the excess current of the device was 5.57 μA under a light intensity of 0.92 mW cm^{-2} when applying a bias voltage of only 1 mV. As we gradually decreased the light density of the contact aligner, however, we observed distortion of the image, or even the absence of any patterns, in the photoresist after development. Figure 7d displays the results of the photoresist exposed at a low power density of 5.5 nW cm^{-2} (or 16 pW cm^{-2}) with an exposure time of 600 s. After development, the photoresist did not record any image during this long exposure times. In contrast, the CdS device could record the power density of the incident light in the form of an electrical readout. Figure 7e reveals that the excess current of the device was approximately 15 nA under a light intensity of 5.5 nW cm^{-2} when applying a bias voltage of 1 mV. Similarly, the excess current of the treated device was approximately 3.1 μA under a light intensity of 16 pW cm^{-2} when applying a bias voltage of 1 V (Figure 7f). Thus, the laser-treated CdS device could immediately measure extremely low power densities of UV light with low power consumption.

■ CONCLUSION

In summary, we have demonstrated that nanocrystallized CdS can behave as highly sensitive UV photodetectors after treatment with a single shot from a KrF laser. Using the 3D-FDTD approach to simulate the optical behavior within a CdS device, we found that the UV light would be almost completely absorbed in a shallow region beneath the surface of the CdS. The effective absorption depth within the CdS film in the visible regime is, however, much deeper than that in the UV regime. The PL signals and Raman spectra of the CdS films provided evidence, which the degree of crystallization of the CdS films increased significantly, with defects also removed effectively, after treatment with a single shot from the KrF laser, confirming the TEM observations. Notably, the excess photocurrents from the CdS devices also increased significantly, even after laser treatment at a power density of only 14 mJ cm^{-2}. Moreover, we observed greater enhancements in responsivity of the laser-treated CdS devices in the UV regime because the absorption area within the CdS film in the UV regime overlapped with the major region of crystal structure transformation. When illuminating the treated CdS device with UV light at a power density of 1.9 nW cm^{-2}, we observed a high responsivity of 74.7 A W^{-1} and a detectivity of 1.0×10^{14} Jones when biasing the device at only 1 mV. Under a bias voltage of 1 V, we obtained a high responsivity of 7.3×10^5 A W^{-1} and a high detectivity of 3.5×10^{16} Jones under an extremely low power density of 16 pW cm^{-2} of UV light. Notably, because the active area of the device was 0.22 cm^2, the light power irradiated on the device was only 3.5 pW. In addition, we found that the measured rise and decay times of the treated devices were only approximately 40 and 70 ms, respectively—much faster than those of ZnO-based UV photodetectors. Therefore, the strategy proposed herein has great potential for application in the development of CdS photoconductors for picowatt−level detection of UV light with low power consumption.

■ ASSOCIATED CONTENT

Supporting Information

Methods, the schematic representation of optical simulation setup, the responsivities of treated CdS device and those of untreated one under illumination with light power density in the range between 5 μW cm^{-2} and 1.9 mW cm^{-2}, the electrical characteristics of CdS devices at a wavelength of 320 nm, the response time of CdS device, and the stability and reproducibility of the treated CdS devices. This material is available free of charge via the Internet at http://pubs.acs.org.

■ AUTHOR INFORMATION

Corresponding Authors

* E-mail: (H.-L. Chen) hsuenlichen@ntu.edu.tw.
*E-mail: (Y.-S. Lai) yslai@narl.ndl.org.tw.

Notes

The authors declare no competing financial interest.

■ ACKNOWLEDGMENTS

We thank the Ministry of Science and Technology, Taiwan, for supporting this study under contracts 103-2221-E-002-041-MY3 and 103-2221-E-002-092-MY3. We also thank Prof. Lon Alex Wang from Graduate Institute of Photonics and Optoelectronics at National Taiwan University for providing the KrF excimer laser and technical assistance.

REFERENCES

(1) Hatch, S. M.; Briscoe, J.; Dunn, S. A Self-Powered ZnO-Nanorod/CuSCN UV Photodetector Exhibiting Rapid Response. *Adv. Mater.* **2013**, *25*, 867−871.
(2) Tsai, D. S.; Lin, C. A.; Lien, W. C.; Chang, H. C.; Wang, Y. L.; He, J. H. Ultra-High-Responsivity Broadband Detection of Si Metal Semiconductor Metal Schottky Photodetectors Improved by ZnO Nanorod Arrays. *ACS Nano* **2011**, *5*, 7748−7753.
(3) Yang, Q.; Guo, X.; Wang, W.; Zhang, Y.; Xu, S.; Lien, D. H.; Wang, Z. L. Enhancing Sensitivity of a Single ZnO Micro-/Nanowire Photodetector by Piezo-Phototronic Effect. *ACS Nano* **2010**, *4*, 6285−6291.
(4) Ates, E. S.; Kucukyildiz, S.; Unalan, H. E. Zinc Oxide Nanowire Photodetectors with Single-Walled Carbon Nanotube Thin-Film Electrodes. *ACS Appl. Mater. Interfaces* **2012**, *4*, 5142−5146.
(5) Zhu, H.; Shan, C. X.; Wang, L. K.; Zheng, J.; Zhang, J. Y.; Yao, B.; Shen, D. Z. Metal-Oxide-Semiconductor-Structured MgZnO Ultraviolet Photodetector with High Internal Gain. *J. Phys. Chem. C* **2010**, *114*, 7169−7172.
(6) Liebler, D. C. The Poisons Within: Application of Toxicity Mechanisms to Fundamental Disease Processes. *Chem. Res. Toxicol.* **2006**, *19*, 610−612.
(7) Helbert, J. N. *Handbook of VLSI Microlithography*, 2nd ed; Noyes Publications/William Andrew: New York, 2001.
(8) Omnès, F.; Monroy, E.; Muñoz, E.; Reverchon, J. L. Wide Bandgap UV Photodetectors: A Short Review of Devices and Applications. *Proc. SPIE* **2007**, *6473*, 64730E.
(9) Koda, Y.; Kuroda, R.; Nakazawa, T.; Nakao, Y.; Sugawa, S. A UV Si−Photodiode with Almost 100% Internal Q.E. and High Transmittance On-Chip Multilayer Dielectric Stack. *Proc. SPIE* **2013**, *8659*, 86590J.
(10) Lin, T. S.; Lee, C. T. Performance Investigation of P−I−N ZnO-Based Thin Film Homojunction Ultraviolet Photodetectors. *Appl. Phys. Lett.* **2012**, *101*, 221118.
(11) Li, Z.; Nayak, B. K.; Iyengar, V. V.; McIntosh, D.; Zhou, Q.; Gupta, M. C.; Campbell, J. C. Laser-Textured Silicon Photodiode with Broadband Spectral Response. *Appl. Opt.* **2011**, *50*, 2508−2511.
(12) Lin, K. T.; Tseng, S. C.; Chen, H. L.; Lai, Y. S.; Chen, S. H.; Tseng, Y. C.; Chu, T. W.; Lin, M. Y.; Lu, Y. P. Ultrahigh-Sensitivity CdS Photoconductors with Instant Response and Ultralow Power Consumption for Detection in Low-Light Environments. *J. Mater. Chem. C* **2013**, *1*, 4244−4251.
(13) Konstantatos, G.; Levina, L.; Fischer, A.; Sargent, E. H. Engineering the Temporal Response of Photoconductive Photodetectors via Selective Introduction of Surface Trap States. *Nano Lett.* **2008**, *8*, 1446−1450.
(14) Li, X.; Carey, J. E.; Sickler, J. W.; Pralle, M. U.; Palsule, C.; Vineis, C. J. Silicon Photodiodes with High Photoconductive Gain at Room Temperature. *Opt. Express* **2012**, *20*, 5518.
(15) Palik, E. D. *Handbook of Optical Constants of Solids*; Academic Press: San Diego, 1998.
(16) Yan, F.; Xin, X.; Aslam, S.; Zhao, Y.; Franz, D.; Zhao, J. H.; Weiner, M. 4H−SiC UV Photo Detectors with Large Area and Very High Specific Detectivity. *IEEE J. Quantum Electron.* **2004**, *40*, 1315−1320.
(17) Mandal, L.; Deo, M.; Yengantiwar, A.; Banpurkar, A.; Jog, J.; Ogale, S. A Quasi−Liquid Iontronic−Electronic Light−Harvesting Hybrid Photodetector with Giant Response. *Adv. Mater.* **2012**, *24*, 3686−3691.
(18) Hu, L.; Yan, J.; Liao, M.; Xiang, H.; Gong, X.; Zhang, L.; Fang, X. An Optimized Ultraviolet−A Light Photodetector with Wide-Range Photoresponse Based on ZnS/ZnO Biaxial Nanobelt. *Adv. Mater.* **2012**, *24*, 2305−2309.
(19) Ardakani, A. G.; Pazoki, M.; Mahdavi, S. M.; Bahrampour, A. R.; Taghavinia, N. Ultraviolet Photodetectors Based on ZnO Sheets: The Effect of Sheet Size on Photoresponse Properties. *Appl. Surf. Sci.* **2012**, *258*, 5405−5411.
(20) Lin, P.; Yan, X.; Zhang, Z.; Shen, Y.; Zhao, Y.; Bai, Z.; Zhang, Y. Self-Powered UV Photosensor Based on PEDOT:PSS/ZnO Micro/Nanowire with Strain-Modulated Photoresponse. *ACS Appl. Mater. Interfaces* **2013**, *5*, 3671−3676.
(21) Lin, P.; Chen, X.; Yan, X.; Zhang, Z.; Yuan, H.; Li, P.; Zhao, Y.; Zhang, Y. Enhanced Photoresponse of Cu_2O/ZnO Heterojunction with Piezo-Modulated Interface Engineering. *Nano Res.* **2014**, *7*, 860−868.
(22) Wang, X.; Liao, M.; Zhong, Y.; Zheng, J. Y.; Tian, W.; Zhai, T.; Zhi, Chunyi; Ma, Y.; Yao, J.; Bando, Y.; Golberg, D. ZnO Hollow Spheres with Double-Yolk Egg Structure for High−Performance Photocatalysts and Photodetectors. *Adv. Mater.* **2012**, *24*, 3421−3425.
(23) Jiang, P.; Jie, J.; Yu, Y.; Wang, Z.; Xie, C.; Zhang, X.; Wu, C.; Wang, Li; Zhu, Z.; Luo, L. Aluminium-Doped N-Type ZnS Nanowires as High-Performance UV and Humidity Sensors. *J. Mater. Chem.* **2012**, *22*, 6856−6861.
(24) Konstantatos, G.; Clifford, J.; Levina, L.; Sargent, E. H. Sensitive Solution-Processed Visible-Wavelength Photodetectors. *Nat. Photonics* **2007**, *1*, 531−534.
(25) Neamen, D. A. *Semiconductor Physics and Devices*, 3rd ed; McGraw−Hill: New York, 2003.
(26) Li, L.; Wu, P.; Fang, X.; Zhai, T.; Dai, Lun; Liao, M.; Koide, Y.; Wang, H.; Bando, Y.; Golberg, D. Single-Crystalline CdS Nanobelts for Excellent Field-Emitters and Ultrahigh Quantum-Efficiency Photodetectors. *Adv. Mater.* **2010**, *22*, 3161−3165.
(27) Heo, K.; Lee, H.; Park, Y.; Park, J.; Lim, H. J.; Yoon, D.; Lee, C.; Kim, M.; Cheong, H.; Park, J.; Jian, J.; Hong, S. Aligned Networks of Cadmium Sulfide Nanowires for Highly Flexible Photodetectors with Improved Photoconductive Responses. *J. Mater. Chem.* **2012**, *22*, 2173−2179.
(28) Repins, I.; Contreras, M. A.; Egaas, B.; DeHart, C.; Scharf, J.; Perkins, C. L.; To, B.; Noufi, R. 19.9%-Efficient ZnO/CdS/$CuInGaSe_2$ Solar Cell with 81.2% Fill Factor. *Prog. Photovoltaics* **2008**, *16*, 235−239.
(29) Fan, Z.; Razavi, H.; Do, J.; Moriwaki, A.; Ergen, O.; Chueh, Y. L.; Leu, P. W.; Ho, J. C.; Takahashi, T.; Reichertz, L. A.; Neale, S.; Yu, K.; Wu, M.; Ager, J. W.; Javey, A. Three-Dimensional Nanopillar-Array Photovoltaics on Low-Cost and Flexible Substrates. *Nat. Mater.* **2009**, *8*, 648−653.
(30) Lee, Y. L.; Lo, Y. S. Highly Efficient Quantum-Dot-Sensitized Solar Cell Based on Co-sensitization of CdS/CdSe. *Adv. Funct. Mater.* **2009**, *19*, 604−609.
(31) Potlog, T.; Ghimpu, L.; Gashin, P.; Pudov, A.; Nagle, T.; Sites, J. Influence of Annealing in Different Chlorides on the Photovoltaic Parameters of CdS/CdTe Solar Cells. *Sol. Energy Mater. Sol. Cells* **2003**, *80*, 327−334.
(32) Goto, F.; Shirai, K.; Ichimura, M. Defect Reduction in Electrochemically Deposited CdS Thin Films by Annealing in O_2. *Sol. Energy Mater. Sol. Cells* **1998**, *50*, 147−153.
(33) Ramaiah, K. S.; Pilkington, R. D.; Hill, A. E.; Tomlinson, R. D.; Bhatnagar, A. K. Structural and Optical Investigations on CdS Thin Films Grown by Chemical Bath Technique. *Mater. Chem. Phys.* **2001**, *68*, 22−30.
(34) ALLGUY, Ltd; http://www.newtouch.com.tw/ (September 2013).
(35) Tsai, C. T.; Chuu, D. S.; Chen, G. L.; Yang, S. L. Studies of Grain Zize Effects in RF Sputtered CdS Thin Films. *J. Appl. Phys.* **1996**, *79*, 9105−9109.
(36) Chuu, D. S.; Dai, C. M.; Hsieh, W. F.; Tsai, C. T. Raman Investigations of the Surface Modes of the Crystallites in CdS Thin Films Grown by Pulsed Laser and Thermal Evaporation. *J. Appl. Phys.* **1991**, *69*, 8402−8404.
(37) Prabhu, R. R.; Khadar, M. A. Study of Optical Phonon Modes of CdS Nanoparticles Using Raman Spectroscopy. *Bull. Mater. Sci.* **2008**, *31*, 511−515.
(38) Gong, X.; Tong, M.; Xia, Y.; Cai, W.; Moon, J. S.; Cao, Y.; Yu, G.; Shieh, C. L.; Nilsson, B.; Heeger, A. J. High-Detectivity Polymer Photodetectors with Spectral Response from 300 to 1450 nm. *Science* **2009**, *325*, 1665−1667.
(39) Soci, C.; Zhang, A.; Xiang, B.; Dayeh, S. A.; Aplin, D. P. R.; Park, J.; Bao, X. Y.; Lo, Y. H.; Wang, D. ZnO Nanowire UV

Photodetectors with High Internal Gain. *Nano Lett.* **2007**, *7*, 1003−1009.
(40) Li, D.; Sun, X.; Song, H.; Li, Z.; Chen, Y.; Jiang, H.; Miao, G. Realization of a High-Performance GaN UV Detector by Nano-plasmonic Enhancement. *Adv. Mater.* **2012**, *24*, 845−849.
(41) Butun, B.; Tut, T.; Ulker, E.; Yelboga, T.; Ozbay, E. High-Performance Visible-Blind GaN-Based P−I−N Photodetectors. *Appl. Phys. Lett.* **2008**, *92*, 033507.